OPEN

NPG Asia Materials (2015) 7, e216; doi:10.1038/am.2015.102

www.nature.com/am

ORIGINAL ARTICLE

Period-doubling reconstructions of semiconductor partial dislocations

Ji-Sang Park[1], Bing Huang[1,2], Su-Huai Wei[1], Joongoo Kang[1,3] and William E McMahon[1]

Atomic-scale understanding and control of dislocation cores is of great technological importance, because they act as recombination centers for charge carriers in optoelectronic devices. Using hybrid density-functional calculations, we present period-doubling reconstructions of a 90° partial dislocation in GaAs, for which the periodicity of like-atom dimers along the dislocation line varies from one to two, to four dimers. The electronic properties of a dislocation change drastically with each period doubling. The dimers in the single-period dislocation are able to interact, to form a dispersive one-dimensional band with deep-gap states. However, the inter-dimer interaction for the double-period dislocation becomes significantly reduced; hence, it is free of mid-gap states. The Ga core undergoes a further period-doubling transition to a quadruple-period reconstruction induced by the formation of small hole polarons. The competition between these dislocation phases suggests a new passivation strategy via population manipulation of the detrimental single-period phase.
NPG Asia Materials (2015) **7,** e216; doi:10.1038/am.2015.102; published online 18 September 2015

INTRODUCTION

Dislocations generally degrade the optoelectronic properties of III–V optoelectronic devices such as light-emitting diodes and solar cells. III–V multijunction solar cells have attained efficiencies in excess of 44%,[1–4] and have the potential to reach efficiencies in excess of 50%.[5] However, many of these device architectures rely on lattice-mismatched epitaxy, for which threading dislocations are inevitable. Because these dislocations act as recombination centers for charge carriers[6–8] and reduce the device efficiency, the density of dislocations in the active region of the device must be minimized, generally by carefully varying the lattice constant in a thick graded layer.[9–11] It may also be possible to mitigate the impact of these dislocations via passivation with impurities,[12–15] or by controlling the type[16] or direction of the remaining dislocations.

A full dislocation may dissociate into two partial dislocations to lower its formation energy.[17–19] All possible structural permutations for glissile $<110>$ dislocations in a III–V crystal are illustrated by the dislocation loop shown in Figure 1.[20] Dissociation into partial dislocations creates two partial dislocation loops separated by a stacking fault. The angle between the partial Burgers vectors (dashed arrows) and the line direction for all segments is either 30° or 90°, and the vector sum of the partial dislocation pairs always equals the Burgers vector of the full dislocation (solid arrow). By definition, an unreconstructed dislocation disrupts the bulk crystal structure and any edge component creates dangling bonds. A second descriptor, 'α' or 'β', in Figure 1 indicates whether these dangling bonds are for group V or group III atoms, respectively. Because these dangling bonds are energetically unfavorable, a dislocation core generally reconstructs to form like-atom dimer bonds. A 90° partial dislocation reconstructs with dimers angled away from the dislocation line direction. There are two well-established reconstructions with similar formation energies, referred to as 'single period' (SP) and 'double period' (DP) based on their periodicity along the dislocation line.[20–25] A 30° partial dislocation reconstructs with dimers aligned parallel to the dislocation line direction.[20,24,26] An atomic model for each of these reconstructions is shown in Figure 2.

A reconstructed dislocation along a high-symmetry crystal direction can be regarded as a one-dimensional extended defect consisting of like-atom dimers repeated along the dislocation line. For some dislocations (for example, 90° SP), the distance between the dimers is not much longer than the dimer bond length itself. Thus, such a one-dimensional extended defect differs from a point defect in that the constituent like-atom dimers may strongly interact with each other. Nonetheless, previous theoretical work[15] neglected the interaction between the dimers. Here we show that these interactions have a fundamental role in determining a dislocation's electronic and atomic structure.

We performed hybrid density-functional theory (DFT) calculations of a 90° partial dislocation in GaAs, to investigate how the inter-dimer interaction affects its structural and electronic properties. For

[1]National Renewable Energy Laboratory, Golden, CO, USA; [2]Oak Ridge National Laboratory, Oak Ridge, TN, USA and [3]Department of Emerging Materials Science, DGIST, Daegu, Korea
Correspondence: Professor J Kang, Department of Emerging Materials Science, DGIST, 333. Techno jungang-daero, Hyeonpung-myeon, Dalseong-gun, Daegu 711-873, Republic of Korea.
E-mail: joongoo.kang@dgist.ac.kr
or Dr WE McMahon, National Renewable Energy Laboratory, 15013 Denver W Pkwy, Golden, CO 80401, USA.
E-mail: bill.mcmahon@nrel.gov
Received 19 March 2015; revised 13 June 2015; accepted 13 July 2015

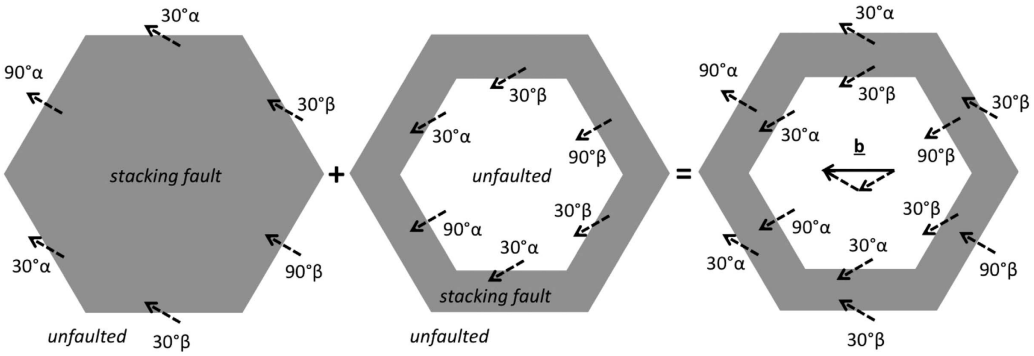

Figure 1 Sequence illustrating how the fundamental glissile dislocations in a III–V crystal are formed from partial dislocations. The plane of the figure is {111} and the edges of the hexagons are <110> directions. (Left) The crystal above the gray hexagon shifts with respect to unfaulted crystal in the direction of the associated partial dislocation (dashed arrows). A hexagonal partial dislocation loop forms, enclosing a (planar) stacking fault. The identity of each of the six partial dislocation segments is determined by the angle between the partial dislocation Burgers vector and the line direction of each segment. (Middle) The crystal above white hexagon shifts (in a different direction) with respect to gray hexagon, returning the enclosed area to an unfaulted stacking sequence. The six partial dislocation segments are once again labeled according to the angle between the partial Burgers vector and the line direction of each segment. (Right) If the pairs of partial dislocations are summed for each segment, they form the following full dislocations with the Burgers vector shown with a solid arrow: (clockwise from the top) screw, 60° β, 60° β, screw, 60° α, and 60° α. Atomic structures for reconstructed partial dislocations are shown in Figure 2. Adapted from reference 20.

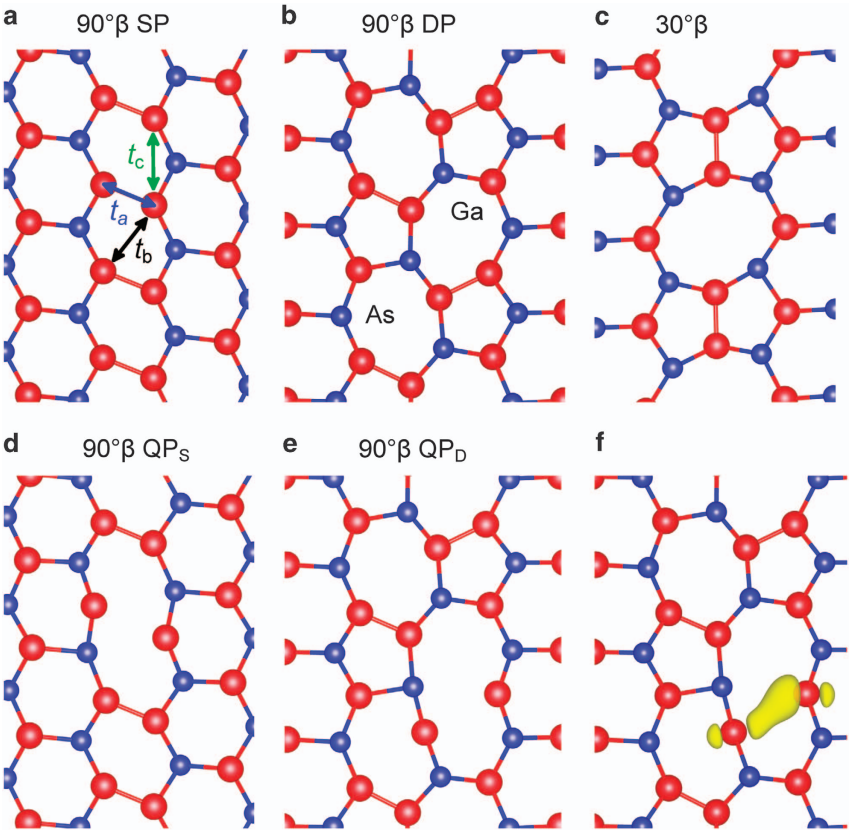

Figure 2 Atomic structures of 90° and 30° partial dislocations. (**a**–**e**) β-Type dislocation reconstructions with Ga–Ga dimers along the dislocation lines. The vertical dislocation line is along the [1–10] direction. α-Type dislocations are topologically same as β-type dislocations, except that the positions of Ga and As atoms are exchanged. The relaxed structures of 90°α SP, 90°α DP and 30°α are presented in Supplementary Figure S1. In **a**, the hopping interactions between the dangling bonds are denoted. (**f**) Charge density plot of the small polaron state for 90°β QP_D, with a contour value of 0.030 $|e|/Å^3$.

comparison, the calculation results for a 30° partial dislocation are also presented. Despite previous DFT studies of the SP and DP reconstructions of a 90° partial dislocation, there still remains large uncertainty in the resulting defect-level positions with respect to the band edges because of the underestimated DFT bandgap. To overcome this, we used hybrid density functional proposed by Heyd, Scuseria and Ernzerhof (HSE) for the exchange correlation.[27] In addition to the SP and DP reconstructions, we propose a 'quadruple-period' (QP) reconstruction as a new ground state for a neutral 90°β-dislocation in GaAs (Figures 2d and e), which contains small polarons of holes that are uniformly distributed along the dislocation line. As we will show later, the inter-dimer interactions in the SP, DP and QP

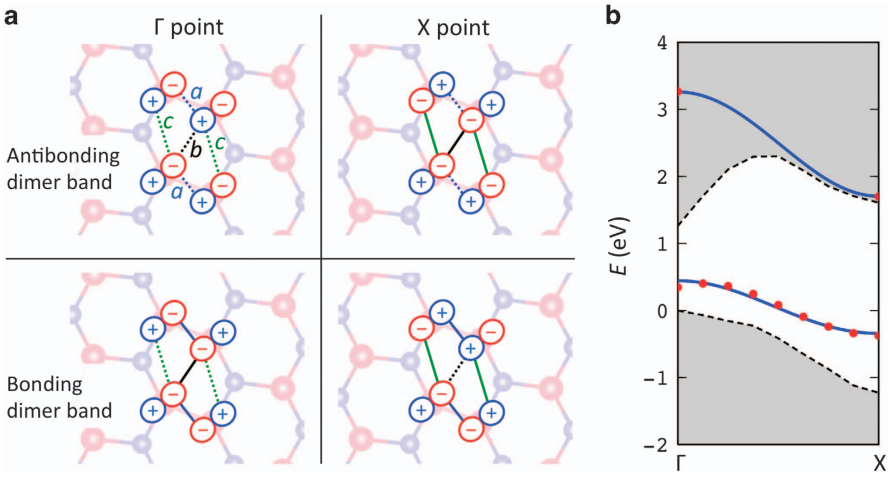

Figure 3 Inter-dimer interactions in a 90° β SP dislocation. (**a**) *p*-Like db orbitals at the dimerized Ga atoms for the antibonding dimer band (upper panels) and the bonding dimer band (bottom panels). The sign on each lobe of a db orbital denotes the relative phase, which is determined by the bonding nature of the Ga–Ga dimer bond and the Bloch phase at a give *k* point. For example, for the antibonding dimer bond at $k=X$ (upper right), the two lobes of the dbs connected by a blue dotted line should be out of phase to form the *a*-type antibonding dimer bond. As the Bloch phase is π at $k=X$, two neighboring *p*-like orbitals at the same side with respect to the vertical dislocation line should have the opposite signs. The relative phases of the db orbitals determine the bonding character of the inter-dimer bonds, as denoted by a solid line for a *p*–*p* bonding interaction and a dotted line for a *p*–*p* antibonding interaction. (**b**) Tight-binding electronic band structure of the defect bands. The hybrid DFT results (dots) were used to fit the tight-binding parameters. The shaded areas represent the valence and conduction bands of GaAs.

reconstructions are quite different and the electronic properties of a dislocation therefore depend strongly on which reconstruction it adopts.

MATERIALS AND METHODS

First-principles calculations of partial dislocations

We performed first-principles density functional calculations to investigate the stability and electronic structure of partial dislocation cores in GaAs, using the Vienna *ab-initio* Simulation Package.[28] We used the HSE hybrid density functional[27] for the exchange correlation and the projector-augmented wave method.[29] The atomic structures were optimized until the residual forces were <0.05 eV Å^{-1}. The optimized lattice constant and the band gap are 5.67 Å and 1.37 eV for bulk GaAs, respectively, close to the experiment values of 5.65 Å and 1.42 eV, respectively.

Our supercells contain two different partial dislocation cores, α and β, to make the sum of the two partial Burger's vectors equal to zero, so as to give the periodic boundary conditions used in our supercell calculations. The two partial dislocations are separated by a stacking fault. To prevent charge transfer between the cores in a supercell, we passivated one of the cores by attaching pseudo-hydrogen atoms. Ga and As dangling bonds are passivated by pseudo hydrogen with 5/4 and 3/4 *e*, respectively.

RESULTS

We first discuss the inter-dimer interaction in the 90° SP α- and β-cores. The 90° SP dislocation is a line defect embedded in GaAs, in which the like-atom dimers are 'polymerized' through electron hopping between the adjacent dimers. The two hopping parameters, t_b and t_c, describe the inter-dimer interaction, while the intra-dimer hopping parameter t_a describes the strength of the dimer bond (Figure 2a). For crystal momentum k, the Bloch Hamiltonian $H(k)$ is given by

$$H(k)=\begin{pmatrix}\varepsilon_{db}+2t_c\cos(kd) & t_a+t_be^{ikd}\\ t_a+t_be^{-ikd} & \varepsilon_{db}+2t_c\cos(kd)\end{pmatrix},$$

where d is the lattice constant along the dislocation line and ε_{db} is the energy of the dangling bond (db) basis state at the core. The defect band structure $\varepsilon_{\pm}(k)$ is given by $\varepsilon_{\pm}(k)=\varepsilon_{db}+2t_c\cos(kd)\pm\sqrt{t_a^2+t_b^2+2t_at_b\cos(kd)}$. Hereafter, the two bands, $\varepsilon_+(k)$ and $\varepsilon_-(k)$, which are well separated in energy by roughly $2|t_a|$, are referred to as the antibonding dimer band and the bonding dimer band, respectively.

The signs of the hopping parameters in $H(k)$, as well as their sizes, essentially determine the dispersion of a dislocation band. The signs of t_a, t_b and t_c are determined by the following considerations.

Figure 3a depicts the *p*-like db orbitals of the 90°β SP dislocation for the dimer bands at $k=\Gamma$ and X. It is interesting to note that the db orbitals are tilted relative to the dimer bond direction, as confirmed by the charge-density plots in Supplementary Figure S2. The sign on each lobe of the db orbitals denotes the relative phase between the lobes. Depending on the hopping parameters involved in the db coupling, there are three different types of bonds, *a*-, *b*- and *c*-types, as denoted in Figure 3a (upper left). The solid (dotted) line represents a *p*–*p* bonding (antibonding) interaction between a selected pair of db orbitals. When two lobes connected by a bond line are in phase, the corresponding bonding state has a *p*–*p* bonding character. On the other hand, for the lobes with the opposite phases, the bonding state has a *p*–*p* antibonding character. By definition, the antibonding dimer band is characterized by the *a*-type antibonding state (blue dotted lines, upper panels), while the bonding dimer band is in the *a*-type bonding state (lower panels). The sign of t_a depends on the choice of the db basis states. We select the db orbitals in the upper left panel as our basis states, so that t_a is positive. It is worth noting that for the antibonding dimer band at $k=\Gamma$, there are two *c*-type antibonding bonds and one *b*-type antibonding bond per unit cell (upper left), whereas at $k=X$, all of these inter-dimer bonds have a bonding character (upper right). From the dispersion relation, the energies of the corresponding states are $\varepsilon_+(\Gamma)=\varepsilon_{db}+t_a+2t_c+t_b$ and $\varepsilon_+(X)=\varepsilon_{db}+t_a-2t_c-t_b$. Therefore, the t_b and t_c should be positive to obtain the right band dispersion.

The tight-binding band structure of 90°β SP is shown in Figure 3b, with the hopping parameters $t_a=1.22$ eV, $t_b=0.19$ eV and $t_c=0.29$ eV, which are fitted to the HSE energy values. The db energy ε_{db} is

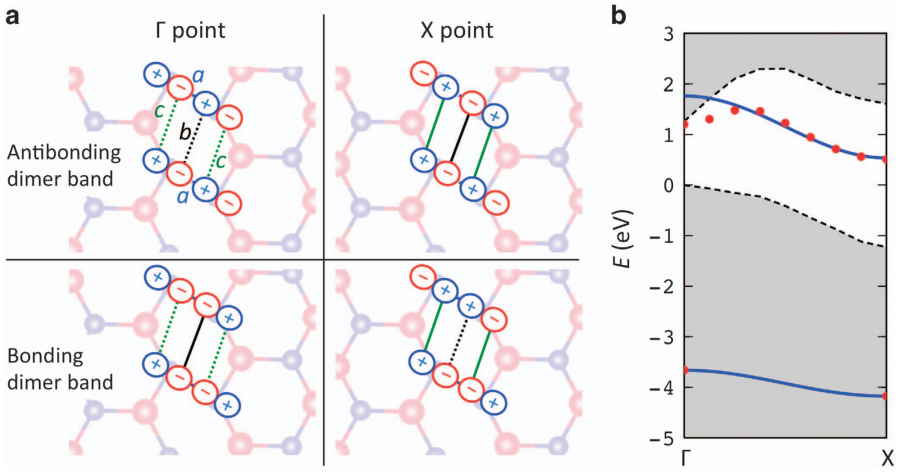

Figure 4 Inter-dimer interactions in a 90° α SP dislocation. (**a**) *p*-Like db orbitals at the dimerized As atoms for the antibonding dimer band (upper panels) and the bonding dimer band (bottom panels). (**b**) Tight-binding electronic band structure of the defect bands. The hybrid DFT results (dots) were used to fit the tight-binding parameters. For the antibonding dimer band, the HSE band energy deviates noticeably from the tight-binding result near the Γ point due to the contribution of the conduction band states.

1.27 eV with respect to the valence band maximum (VBM) of GaAs. Although the bonding dimer band is less dispersive than the antibonding dimer band, owing to the mixed nature of the inter-dimer bonds, the inter-dimer interactions, parameterized by t_b and t_c, are responsible for the deep-gap states of the 90° β SP near the Γ point.

Similarly, for the 90° α SP dislocation, we found that the inter-dimer interaction leads to a dispersive antibonding dimer band, creating deep-gap states near the *X* point (Figure 4). In this case, the hopping parameters are $t_a = 2.54$ eV, $t_b = 0.18$ eV and $t_c = 0.22$ eV. The db energy ε_{db} is -1.39 eV with respect to the VBM. Unlike in the case of the β core, the *p*-like db orbitals in the α-core are conventional in the sense that they are oriented along the dimer bond direction (Figure 4 and Supplementary Figure S3). Consequently, the dimerization energy, which is proportional to t_a, is much larger for the α-core than for the β-core. In addition to the 'conventional' db states, we note that there exist other *p*-like db states in the α-core (Supplementary Figure S4), for which the *p*-like orbitals are tilted relative to the dimer bond direction. However, these db states are 'hidden' inside the GaAs bands and thus are not detrimental to the optoelectronic properties of GaAs.

Figures 5a and b show the projected density of states (PDOS) for the 90° SP β- and α-cores, respectively. The PDOS of the β-core close to the VBM is derived from the Ga–Ga bonding dimer band, whereas the PDOS of the α-core close to the conduction band minimum is from the As–As antibonding dimer band. The interaction among the dimers is responsible for the broad PDOS. The two peaks in the PDOS are due to the dispersion of the defect band, which is relatively flat at $k = \Gamma$ and *X*. It is noteworthy that the dispersive defect band is partially occupied by residual electrons or holes (Figures 5a and b). For the neutral β-core, each Ga db contributes 3/4 electrons and the bonding dimer band is occupied by 0.5 hole per dimer. For the neutral α-core, each As db contributes 5/4 electrons and the antibonding dimer band is thus occupied by 0.5 electron per dimer.

For the 90° DP reconstruction in Figure 2b, dimers along the dislocation line are spatially separated and no mid-gap states are expected due to significantly weakened inter-dimer interaction. Indeed, the PDOS of 90° DP in Figures 5c and d exhibit shallower, less-dispersive defect bands than those of the SP dislocations. Likewise, we obtained the nearly dispersionless PDOS for the 30° β- and α-cores (Figures 5g and h), for which the inter-dimer interaction is negligible due to the large separation between the dimers (Figure 2c). In the 90° DP and 30° reconstructions, the dimers behave more like isolated dimers. As in the case of SP, each Ga–Ga bond has 0.5 residual holes in the bonding dimer state, whereas each As–As dimer has 0.5 residual electrons in the antibonding dimer state.

Our HSE calculations show that the formation energies of the 90° SP and DP of GaAs are very similar, partly because the density of dimers along the dislocation line is similar. For the neutral 90° β-core, the formation energy of the SP is 0.034 eV per dimer lower than that of the DP. For the neutral 90° α-core, their stability is reversed and the DP is 0.044 eV per dimer more stable than the SP. Here we point out two factors that determine their stability. First, the residual carriers in the defect states have a critical role in the competition between SP and DP. For the 90° β SP, the residual holes occupy the top of the bonding dimer band near the Γ point (Figure 3b), at which the *c*-type inter-dimer bonds have an antibonding character. For the 90° α SP, the residual electrons occupy the bottom of the antibonding dimer band near the *X* point (Figure 4b), which has the inter-dimer bonding character. Therefore, in both cases the inter-dimer interaction mediated by residual carriers increases the relative stability of SP. On the other hand, when the DP is formed, the strain accumulated in the SP core is released through the bond rearrangement, enhancing the relative stability of DP. These two effects are nearly balanced, so that the formation energies of SP and DP are similar.

Next, we show that despite containing broken dimer bonds, a novel QP reconstruction is even more stable than the SP and DP phases for a neutral 90° β partial dislocation in GaAs. There are two types of QP that can be derived from SP and DP (Figures 2d and e). These two QP phases are referred to as QP_S and QP_D. The QP_D is 0.149 eV more stable than the SP per dimer, and it is slightly more stable than the QP_S by 0.016 eV per dimer. The key to explaining the stability of QP is to understand the different hole distributions in the DP (or SP) and the QP. As discussed earlier, for 90° β DP or SP, the holes in the bonding dimer states are delocalized over the dimers along the dislocation line with 0.5 hole per dimer on average. However, the delocalized hole state turns out to be unstable in the presence of the hole–lattice interactions. For 90° β QP, the hole polarizes or deforms its surrounding lattice in a way that the two holes in the unit cell become localized around a single Ga–Ga dimer, so that the rest of the shallow bonding dimer states near the VBM can be fully occupied, thus lowering the total energy. In this case, one of the four dimer

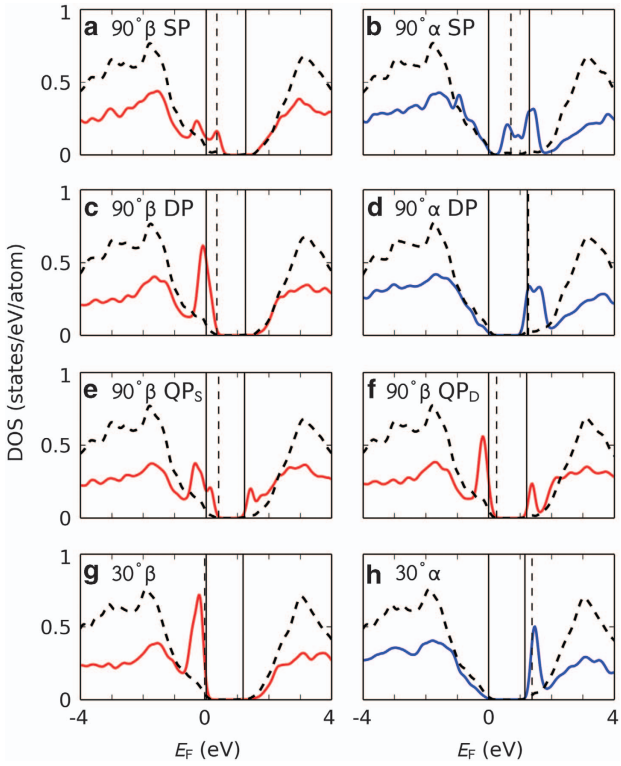

Figure 5 Electronic properties of 90° partial dislocations with various reconstruction periodicities. (**a**–**f**) The PDOS of a 90° partial dislocation phases are presented in a period-doubling sequence of SP, DP and QP. (**g** and **h**) The PDOS of 30° partial dislocations are also shown for comparison. In each figure, a solid line represents the PDOS of dimerized Ga or As atoms, and dashed lines represent the total DOS normalized by the number of atoms in the supercell. The vertical solid lines denote the VBM and the conduction band minimum (CBM), and the VBM is set to 0 eV. The vertical dashed line denotes the Fermi energy.

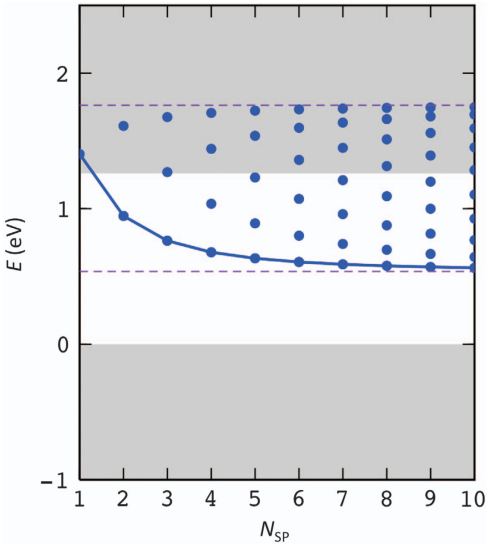

Figure 6 Defect states of a finite SP segment in a 90° α dislocation. Tight-binding energy levels of the antibonding dimer states as a function of the number of SP dimers (N_{SP}) in the segment. The tight-binding Hamiltonian of the SP segment is constructed from the db energy and the hopping parameters of the pure SP (see the text in the Supplementary Information). The horizontal dashed lines denote the band edge positions of the antibonding dimer band of an infinitely long SP phase in Figure 4b.

bonds in the QP_D unit cell is elongated by 50% to trap two holes, forming a small polaron of holes in the dislocation core (Figure 2f). In contrast, the remaining dimer bonds are shortened by 2%. We found that the small polaron state appears in the conduction band of GaAs. The fully occupied bonding dimer states of the remaining dimer bonds appear near the VBM (Figures 5e and f).

We also checked the possibility of the formation of small electron polarons in the 90° α QP core. The excess residual electrons in the antibonding dimer states may be trapped at a single broken As–As dimer in the QP unit cell, forming small electron polarons.[30] However, our HSE calculation shows that the 90° α QP is not stable even as a local minimum structure, which is consistent with the large dimerization energy and the large strain energy associated with the lattice distortion in the As core.

DISCUSSION

The above results contribute to the understanding of recombination at mid-gap states in GaAs. One thing to note is that the results discussed here are limited to perfectly straight dislocations, and that kink sites[22,31–34] or any other imperfections[35–38] neglected here may host mid-gap states. Nonetheless, even perfectly straight, impurity-free, dislocations can exhibit additional structural complexity. Here we will show that a mixture of reconstructions is likely to form at elevated (growth) temperatures, and that this can affect the existence and passivation of mid-gap states.

We have learned that neither of the ground-state reconstructions, 90° α DP and 90° β QP, supports mid-gap states (Figure 5). Deep-gap states appear only when the dimers are coupled to form a dispersive defect band as in the SP. The 90° α SP supports mid-gap states and its energy is only $\Delta E = 0.044$ eV per dimer higher than the ground-state DP. At temperature T, the population of the SP is estimated to be $\rho_{SP} = 1/[1+\exp(2\Delta E/k_B T)]$ within the crude approximation neglecting the boundary energy of the SP–DP mixed phases. In the equation, k_B is the Boltzmann constant, and the factor 2 in front of ΔE is necessary because the DP-to-SP conversion creates two SP dimers per unit cell. From the thermodynamic consideration, the population of the SP phase is $\rho_{SP} = 3.1\%$ at room temperature. At a growth temperature $T = 700$ °C, the SP population would increase to 25.9 %. Because of the small SP population, the chance of having a long SP segment in between the DP regions is small. Then, an important question is whether a relatively short SP segment can support mid-gap states. Using the tight-binding Hamiltonian of a SP segment, we found that a very short SP segment containing just four SP dimers gives mid-gap states nearly as deep as for the pure SP phase (Figure 6). Therefore, the short SP segment in the mixed phase can create deep gap levels and act as a recombination center.

For improved optoelectronic properties, the formation of the SP segments in the 90° α-core should be suppressed by enhancing the stability of DP with respect to SP. Although previous studies only considered neutral dislocations in GaAs,[15,20,24,26] their stability depends on the charge state as shown in Si.[39] For the neutral 90° α, as discussed earlier, the residual electrons occupying the antibonding dimer states are responsible for the enhanced relative stability of SP. Therefore, the energy difference, $\Delta E = E_{SP} - E_{DP}$, can be tuned by changing the electron occupation of the defect states. Indeed, our hybrid DFT calculations of charged dislocation cores show that ΔE increases from 0.044 eV per dimer to 0.247 eV per dimer, as the residual electron of 0.5 electron per dimer is removed. Therefore, the population of the harmful SP minority phase should be substantially reduced by shallow p-type doping of the 90° α-core.

CONCLUSION

Our hybrid DFT calculations establish the SP-, DP- and QP-reconstructed atomic structures of the 90° partial dislocation in GaAs. The electronic properties of the SP and DP are revisited, revealing the nature of the interaction between the constituent dimers of the dislocations. We found that the defect states of the DP are shallow, whereas the inter-dimer interaction in the SP leads to detrimental mid-gap states. Furthermore, for the first time, we report on the formation of small polarons in the 90° β dislocation, which leads to the ground-state QP phase for the neutral 90° β-core. The fundamental understanding of the SP, DP and QP reconstructions suggests a new passivation strategy by biasing the competition between these phases through the tuning of the carrier density in the dislocation. The insights obtained from this study will also help to understand and control other one-dimensional extended defects such as grain boundaries in MoS_2[40] and other two-dimensional semiconductors.

CONFLICT OF INTEREST

The authors declare no conflict of interest.

ACKNOWLEDGEMENTS

The work at NREL was supported by the US Department of Energy, EERE, under contract number DE-AC36-08GO28308. The work at DGIST was supported by the DGIST MIREBraiN Program. We thank Andrew Norman and Ryan France for their helpful discussions.

Author contributions: JSP performed and analyzed theoretical calculations, and contributed to the writing of the manuscript. JK performed and analyzed theoretical calculations, contributed to the writing of the manuscript and the direction of the project. BH performed and analyzed theoretical calculations. SHW developed theoretical methods, analyzed the theoretical calculations, contributed to the writing of the manuscript and the direction of the project. WEM contributed to the atomic structural modeling, the direction of the project and the writing of the manuscript.

1 France, R. M., Geisz, J. F., García, I., Steiner, M. A., McMahon, W. E., Friedman, D. J., Moriarty, T. E., Osterwald, C., Ward, J. S. Design Flexibility of Ultra-High Efficiency 4-Junction Inverted Metamorphic Solar Cells. in *42nd IEEE Photovoltaics Specialists Conference* (New Orleans, 14–19 June 2015) http://www.nrel.gov/news/press/2014/15436.html (2014).
2 Dimroth, F., Tibbits, T. N. D., Niemeyer, M., Predan, F., Beutel, P., Karcher, C., Oliva, E., Siefer, G., Lackner, D., Fuß-Kailuweit, P., Bett, A. W., Krause, R., Drazek, C., Guiot, E., Wasselin, J., Tauzin, A. and Signamarcheix, T. Four-Junction Wafer Bonded Concentrator Solar Cells. in *42nd IEEE Photovoltaics Specialists Conference* (New Orleans, June 14–19 2015). http://www.ise.fraunhofer.de/en/press-and-media/press-releases/press-releases-2014/new-world-record-for-solar-cell-efficiency-at-46-percent (2014).
3 Dimroth, F., Grave, M., Beutel, P., Fiedeler, U., Karcher, C., Tibbits, T. N. D., Oliva, E., Siefer, G., Schachtner, M., Wekkeli, A., Bett, A. W., Krause, R., Piccin, M., Blanc, N., Drazek, C., Guiot, E., Ghyselen, B., Salvetat, T., Tauzin, A., Signamarcheix, T., Dobrich, A., Hannappel, T. & Schwarzburg, K. Wafer bonded four-junction GaInP/GaAs//GaInAsP/GaInAs concentrator solar cells with 44.7% efficiency. *Prog. Photovolt Res. Appl.* **22**, 277–282 (2014).
4 France, R. M., Geisz, J. F., Garcia, I., Steiner, M. A., McMahon, W. E., Friedman, D. J., Moriarty, T. E., Osterwald, C., Ward, J. S., Duda, A., Young, M. & Olavarria, W. J. Quadruple-junction inverted metamorphic concentrator devices. *IEEE J. Photovolt* **5**, 432–437 (2015).
5 Friedman, D. J. Progress and challenges for next-generation high-efficiency multi-junction solar cells. *Curr. Opin. Solid State Mater. Sci.* **14**, 131–138 (2010).
6 Heinke, W. & Queisser, H. J. Photoluminescence at dislocations in GaAs. *Phys. Rev. Lett.* **33**, 1082–1084 (1974).
7 Ross, F. M., Hull, R., Bahnck, D., Bean, J. C., Peticolas, L. J. & King, C. A. Changes in electrical device characteristics during the *in situ* formation of dislocations. *Appl. Phys. Lett.* **62**, 1426–1428 (1993).
8 Giovane, L. M., Luan, H. –C., Agarwal, A. M. & Kimerling, L. C. Correlation between leakage current density and threading dislocation density in SiGe *p-i-n* diodes grown on relaxed graded buffer layers. *Appl. Phys. Lett.* **78**, 541–543 (2001).
9 Fitzgerald, E. A., Xie, Y. -H., Monroe, D., Silverman, P. J., Kuo, J. M., Kortan, A. R., Thiel, F. A. & Weir, B. E. Relaxed Ge_xSi_{1-x} structures for III–V integration with Si and high mobility two-dimensional electron gases in Si. *J. Vac. Sci. Technol. B* **10**, 1807–1819 (1992).
10 Beanland, R., Dunstan, D. J. & Goodhew, P. J. Plastic relaxation and relaxed buffer layers for semiconductor epitaxy. *Adv. Phys.* **45**, 87–146 (1996).
11 France, R. M., Garcia, I., McMahon, W. E., Norman, A. G., Simon, J., Geisz, J. F., Friedman, D. J. & Romero, M. J. Lattice-mismatched 0.7-eV GaInAs solar cells grown on GaAs using GaInP compositionally graded buffers. *IEEE J. Photovoltaic.* **4**, 190–195 (2014).
12 Matragrano, M. J., Watson, G. P., Ast, D. G., Anderson, T. J. & Pathangey, B. Passivation of deep level states caused by misfit dislocations in InGaAs on patterned GaAs. *Appl. Phys. Lett.* **62**, 1417–1419 (1993).
13 Yan, Y., Jiang, C. S., Noufi, R., Wei, S. H., Moutinho, H. R. & Al-Jassim, M. M. Electrically benign behavior of grain boundaries in polycrystalline $CuInSe_2$ Films. *Phys. Rev. Lett.* **99**, 235504 (2007).
14 Zhang, L., Da Silva, J. L., Li, J., Yan, Y., Gessert, T. A. & Wei, S. H. Effect of copassivation of Cl and Cu on CdTe grain boundaries. *Phys. Rev. Lett.* **101**, 155501 (2008).
15 Zhang, L., McMahon, W. E. & Wei, S. -H. Passivation of deep electronic states of partial dislocations in GaAs: a theoretical study. *Appl. Phys. Lett.* **96**, 121912–121913 (2010).
16 Simpkins, B. S., Yu, E.T., Waltereit, P. & Speck, J. S. Correlated scanning Kelvin probe and conductive atomic force microscopy studies of dislocations in gallium nitride. *J. Appl. Phys.* **94**, 1448–1453 (2003).
17 Jones, R. Theoretical calculations of electron states associated with dislocations. *J. Phys. Paris* **40**, 33–38 (1979).
18 Hirsch, P. B. Recent results on the structure of dislocations in tetrahedrally coordinated semiconductors. *J. Phys. Paris* **40**, 27–32 (1979).
19 Hirth, J. P. & Lothe, J. *Theory of Dislocations*, (Krieger Publication Company, Malabar, FL, USA, 1992).
20 Beckman, S. P. & Chrzan, D. C. Structure and energy of the partial dislocation cores in GaAs. *Phys. Stat. Solid. B* **243**, 2122–2132 (2006).
21 Jones, R., Umerski, A., Sitch, P., Heggie, M. I. & Öberg, S. Density functional calculations of the structure and properties of impurities and dislocations in semiconductors. *Phys. Stat. Solid. A* **138**, 369–381 (1993).
22 Bennetto, J., Nunes, R.W. & Vanderbilt, D. Period-doubled structure for the 90° partial dislocation in silicon. *Phys. Rev. Lett.* **79**, 245–248 (1997).
23 Blase, X., Lin, K., Canning, A., Louie, S. G. & Chrzan, D. C. Structure and energy of the 90° partial dislocation in diamond: a combined *ab initio* and elasticity theory analysis. *Phys. Rev. Lett.* **84**, 5780–5783 (2000).
24 Beckman, S. P. & Chrzan, D. C. Dislocation cores and their electronic states: partial dislocations in GaAs. *Phys. B* **340–342**, 1001–1004 (2003).
25 Beckman, S. P. & Chrzan, D. C. Reconstruction energies of partial dislocations in cubic semiconductors. *Phys. Rev. B* **76**, 144110 (2007).
26 Justo, J. F., Antonelli, A. & Fazzio, A. Dislocation core properties in semiconductors. *Solid State Commun.* **118**, 651–655 (2001).
27 Heyd, J., Scuseria, G. E. & Ernzerhof, M. Hybrid functionals based on a screened Coulomb potential. *J. Chem. Phys.* **118**, 8207–8215 (2003).
28 Kresse, G. & Furthmüller, J. Efficient iterative schemes for *ab initio* total-energy calculations using a plane-wave basis set. *Phys. Rev. B* **54**, 11169–11186 (1996).
29 Blöchl, P. E. Projector augmented-wave method. *Phys. Rev. B* **50**, 17953–17979 (1994).
30 Kang, J., Jung, Y. S., Wei, S. -H. & Dillon, A. C. Implications of the formation of small polarons in Li_2O_2 for Li-air batteries. *Phys. Rev. B* **85**, 035210 (2012).
31 Nunes, R. W., Bennetto, J. & Vanderbilt, D. Structure, barriers, and relaxation mechanisms of kinks in the 90° partial dislocation in silicon. *Phys. Rev. Lett.* **77**, 1516–1519 (1996).
32 Nunes, R. W., Bennetto, J. & Vanderbilt, D. Atomic structure of dislocation kinks in silicon. *Phys. Rev. B* **57**, 10388–10397 (1998).
33 Blumenau, A. T., Fall, C. J., Jones, R., Heggie, M. I., Briddon, P. R., Frauenheim, T. & Öberg, S. Straight and kinked 90° partial dislocations in diamond and 3C-SiC. *J. Phys. Condens. Matter* **14**, 12741 (2002).
34 Oyama, N. & Ohno, T. Migration processes of the 30° partial dislocation in silicon. *Phys. Rev. Lett.* **93**, 195502 (2004).
35 Csányi, G., Ismail-Beigi, S. & Arias, T. A. Paramagnetic structure of the soliton of the 30° partial dislocation in silicon. *Phys. Rev. Lett.* **80**, 3984–3987 (1998).
36 Justo, J. F., de Koning, M., Cai, W. & Bulatov, V. V. Vacancy interaction with dislocations in silicon: the shuffle-glide competition. *Phys. Rev. Lett.* **84**, 2172–2175 (2000).
37 Castaldini, A., Cavalcoli, D., Cavallini, A. & Pizzini, S. Experimental evidence of dislocation related shallow states in *p*-type Si. *Phys. Rev. Lett.* **95**, 076401 (2005).
38 Rhode, S. K., Horton, M. K., Kappers, M. J., Zhang, S., Humphreys, C. J., Dusane, R. O., Sahonta, S. & Moram, M. A. Mg doping affects dislocation core structures in GaN. *Phys. Rev. Lett.* **111**, 025502 (2013).
39 de Araújo, M. M., Justo, J. F. & Nunes, R. W. Electronic charge effects on dislocation cores in silicon. *Appl. Phys. Lett.* **85**, 5610–5612 (2004).
40 Zou, X., Liu, Y. & Yakobson, B. I. Predicting dislocations and grain boundaries in two-dimensional metal-disulfides from the first principles. *Nano Lett.* **13**, 253–258 (2012).